Energy Fuels **2010,** *24,* 6018–6033 · DOI:10.1021/ef100930m
Published on Web 11/04/2010

energy&fuels
article

Evaluation of Gas Production Potential from Marine Gas Hydrate Deposits in Shenhu Area of South China Sea

Gang Li,[†] George J. Moridis,[‡] Keni Zhang,[‡] and Xiao-Sen Li*,[†]

[†]*Key Laboratory of Renewable Energy and Gas Hydrate, Guangzhou Institute of Energy Conversion, Chinese Academy of Sciences, Guangzhou 510640, P. R. China, and* [‡]*Lawrence Berkeley National Laboratory, 1 Cyclotron Road, MS 90-1116, Berkeley, California 94720, United States*

Received July 21, 2010. Revised Manuscript Received September 17, 2010

The Shenhu Area is located in the Pearl River Mouth Basin, the northern continental slope of the South China Sea. In 2007, gas hydrate samples were recovered during the scientific expedition conducted by the China Geological Survey in the area. Using numerical simulation and currently available data from site measurements, including the water depth, thickness of the hydrate-bearing layer (HBL), sediment porosity, salinity, and pressures and temperatures at key locations, we developed preliminarily estimates of the production potential of these hydrates as gas-producing resource. We used measurements of ambient temperature in the sediments to determine the local geothermal gradient. Evidence from this and other field studies showed that the initial pressure distribution followed the hydrostatic gradient. Direct measurements from core samples provided estimates of the initial hydrate saturation and of the intrinsic permeabilities in the various strata of the system. The hydrate accumulations in the Shenhu Area appear to be hydrate deposits involving a single HBL within fine-textured sediments and boundaries (overburden and underburden layers) which have the same intrinsic permeabilities with the HBL. We investigated gas production from the Shenhu hydrates by means of depressurization and thermal stimulation using a single horizontal well placed in the middle of the HBL. The simulation results indicated that the hydrates dissociate along cylindrical interfaces around the well and along horizontal dissociation interfaces at the top and bottom of the HBL. Production is invariably lower than that attainable in a confined system, and thermal stimulation is shown to affect only a limited region around the well. The sensitivity analysis demonstrates the dependence of production on the level of depressurization, the initial hydrate saturation, the intrinsic permeability of the HBL, the temperature of the well, and the initial temperature of the HBL. A general observation is that gas production is low and is burdened with significant water production, making the hydrate accumulations at the Shenhu Area unattractive production targets with current technology.

1. Introduction

1.1. Background. Natural gas hydrates (NGH) are solid, nonstoichiometric compounds formed by host water molecules with small guest molecules, such as CH_4, C_2H_6, C_3H_8, CO_2, H_2S, etc.[1] Natural gas hydrate deposits involve mainly CH_4 and occur in the permafrost and in deep ocean sediment, where the necessary conditions of low temperature and high pressure exist for hydrate stability. Recent seismic explorations and geological researches show that natural gas hydrates existing in the sediment constitute a large natural gas reservoir that invites consideration as a potential strategic energy resource.[2,3] Techniques for gas production from hydrate deposit are based on three major dissociation principles, i.e., (1) depressurization,[4−6] involving a pressure P decrease below the dissociation pressure at a given temperature T of the hydrate; (2) thermal stimulation,[7−9] involving raising T above the dissociation temperature at a given P of the hydrate; (3) inhibitor effects,[10] based on the use of chemicals, such as salts and alcohols to shift the hydrate $P-T$ equilibrium. Among these possible methods for hydrate

*To whom correspondence should be addressed. Telephone: +86 20 87057037. Fax: +86 20 87057037. E-mail: lixs@ms.giec.ac.cn.

(1) Sloan, E. D.; Koh, C. A. *Clathrate Hydrates of Natural Gases*, 3rd ed.; CRC Press: Boca Raton, FL, 2008.
(2) Collett, T. S. Gas hydrates as a future energy resource. *Geotimes* **2004**, *49* (11), 24–27.
(3) Klauda, J. B.; Sandler, S. I. Global Distribution of Methane Hydrate in Ocean Sediment. *Energy Fuels* **2005**, *19* (2), 459–470.
(4) Ahmadi, G.; Ji, C. A.; Smith, D. H. Production of natural gas from methane hydrate by a constant downhole pressure well. *Energy Convers. Manage.* **2007**, *48* (7), 2053–2068.
(5) Moridis, G. J.; Kowalsky, M. B.; Pruess, K. Depressurization-induced gas production from class 1 hydrate deposits. *SPE Reservoir Eval. Eng.* **2007**, *10* (5), 458–481.
(6) Li, G.; Li, X. S.; Chen, Q.; Chen, Z. Y. Numerical Studies of Gas Production from Gas hydrate zone in Shenhu Area, South China Sea. *Acta Chim. Sin.* **2010**, *68* (11), 1083–1092.
(7) Li, G.; Tang, L. G.; Huang, C.; Feng, Z.; Fan, S. S. Thermodynamic evaluation of hot brine stimulation for natural gas hydrate dissociation. *J. Chem. Ind. Eng.* (*China*) **2006**, *57* (9), 2033–2038.
(8) Li, G.; Li, X. S.; Tang, L. G.; Li, Q. P. Control Mechanisms for Methane Hydrate Production by Thermal Stimulation. In *The 6th International Conference on Gas Hydrate*, Vancouver, British Columbia, Canada, 2008; Paper 5783.
(9) Li, G.; Moridis, G. J.; Zhang, K.; Li, X. S. The Use of Huff and Puff Method in a Single Horizontal Well in Gas Production from Marine Gas Hydrate Deposits in the Shenhu Area of the South China Sea. In *2010 SPE International Oil & Gas Conference & Exhibition in China*, Beijing, China, 2010; Paper 131160.
(10) Li, G.; Li, X. S.; Tang, L. G.; Zhang, Y. Experimental investigation of production behavior of methane hydrate under ethylene glycol stimulation in unconsolidated sediment. *Energy Fuels* **2007**, *21* (6), 3388–3393.

dissociation for gas production, depressurization appears to be the most efficient.[11−16]

The Blake Ridge hydrate accumulation offshore the Carolinas,[17] in which large volumes of gas hydrate are relatively evenly distributed through vast volumes of fine-grained and relatively undeformed sediment at low (2−4% average, with a maximum estimate of 5−12%) saturations, has been extensively studied since the ocean drilling program (ODP) Leg 164.[18] A preliminary estimate of the gas resource at the Blake Ridge is up to 19.3×10^{12} m^3 (13.7×10^9 t under the standard atmospheric condition).[18] Unfortunately, the prospects for economic recovery of natural gas from this highly disseminated resource in the fine-grained sediment of low permeability are very poor with current technologies.[14,19] However, a numerical simulation indicates that the hydrate accumulations at Blake Ridge with the free gas reservoir beneath the hydrate bearing layer may be of economic value for industry production.[20]

Recent studies[11,12,16] have also indicated that, under certain conditions, gas can be produced from natural hydrate deposits at high rates over long periods using conventional technology based on vertical wells. There are also simulation results from horizontal well studies[13,16] that show significant advantages over vertical wells during production from Class 2 and Class 3 deposits.

1.2. Shenhu Area. Recent studies have documented the occurrence of significant gas hydrate deposits in the Shenhu Area of the South China Sea. The Shenhu Area is located in the near southeast of Shenhu Underwater Sandy Bench in the middle of the north slope of the South China Sea, between Xisha Trough and Dongsha Islands. Tectonically, the research area is located in the Zhu II Depression of the Pearl River Mouth Basin (Figure 1), which has been in the process of tectonic subsidence since the middle Miocene. It is characterized by a high sedimentation rate[21] and thick sediments of 1000−7000 m, with organic matter contents of 0.46−1.9%.[22] The geological and thermodynamic conditions in the Shenhu Area are conducive to the formation and stability of gas hydrates.

1.3. Hydrates in the Shenhu Area. Gas hydrate samples were collected at three sites (SH2, SH3, and SH7) during a recent scientific expedition conducted by the China Geological Survey in the Shenhu area of the northern South China Sea in May 2007.[21,23−26] This was the first indication of abundant hydrates in this area, which raised its visibility as a potentially important area for gas hydrate exploitation in China.

From site measurements that included formation thermal conductivity analysis at 19 sites, the heat flow in the Shenhu Area was estimated to ranges from 74.0 to 78.0 mW/m^2 (with an average of 76.2 mW/m^2). Estimates of the geothermal gradient were based on *in situ* temperature measurements at five drilling sites within the research area (including site SH7, on which this study focuses), and ranged from 43 to 67.7 °C/km. These create thermodynamic conditions that favor the formation of stable gas hydrates. The depth and thickness of the gas hydrate zone are controlled by the T, P, and salinity, with the water temperature at the ocean floor T_{OF} and the geothermal gradient in the sediments being the key parameters. In the South China Sea, T_{OF} is in the 4−5 °C range for water depths exceeding 1 000 m.[21,24]

The drilling results from the hydrate layer in the Shenhu Area, measured from both nonpressure and pressurized cores, indicate that the top of the hydrate layers are located 155−229 m below the seafloor (mbsf), and their thickness varies from 10 to 43 m. These hydrate layers occur at water depths 1108−1245 m. The sediment porosity ϕ and the *in situ* salinity X_S in the Shenhu Area, measured from the pressure cores, are 33−48% and 0.0290−0.0315, respectively; the T_{OF} and X_S at the seafloor are 3.3−3.7 °C and 0.0328−0.0334, respectively. The P-wave velocity and gamma density of pressure cores of the site SH7 used in this study are shown in Table 1. The wire-line logging features of site SH7 were described by Wu et al.,[21,24,25] Zhang et al., [26] and Schultheiss et al.[27]

(11) Moridis, G. J.; Reagan, M. T. Gas Production from Oceanic Class 2 Hydrate Accumulations. In *The Offshore Technology Conference*, Houston, Texas, 2007; Paper OTC 18866.
(12) Moridis, G. J.; Reagan, M. T. Strategies for Gas Production from Oceanic Class 3 Hydrate Accumulations. In *The Offshore Technology Conference*, Houston, Texas, 2007; Paper OTC 18865.
(13) Moridis, G. J.; Reagan, M. T.; Zhang, K. The Use of Horizontal Wells in Gas Production from Hydrate Accumulations. In *The 6th International Conference on Gas Hydrate*, Vancouver, British Columbia, Canada, 2008; Paper 5722.
(14) Moridis, G. J.; Collett, T. S.; Boswell, R.; Kurihara, M.; Reagan, M. T.; Koh, C.; Sloan, E. D. Toward Production from Gas Hydrates: Current Status, Assessment of Resources, and Simulation-Based Evaluation of Technology and Potential. *SPE Reservoir Eval. Eng.* **2009**, *12* (5), 745–771.
(15) Moridis, G. J.; Reagan, M. T.; Kim, S. J.; Seol, Y.; Zhang, K. Evaluation of the Gas Production Potential of Marine Hydrate Deposits in the Ulleung Basin of the Korean East Sea. *SPE J.* **2009**, *14* (4), 759–781.
(16) Kurihara, M.; Funatsu, K.; Ouchi, H.; Masuda, Y.; Narita, H. Investigation on Applicability of Methane Hydrate Production Methods to Reservoirs with Diverse Characteristics. In *The 5th International Conference on Gas Hydrate*, Trondheim, Norway, 2005; Paper 3003.
(17) Borowski, W. S. A review of methane and gas hydrates in the dynamic, stratified system of the Blake Ridge region, offshore southeastern North America. *Chem. Geol.* **2004**, *205* (3−4), 311–346.
(18) Collett, T. S.; Ladd, J. Detection of gas hydrate with downhole logs and assessment of gas hydrate concentrations (saturations) and gas volumes on the Blake Ridge with electrical resistivity log data. In *Proceedings ODP Scientific Results*; Paull, C. K., Matsumoto, R., Wallace, P. J., Dillon, W. P., Eds.; TAMU: College Station, TX, 2000; Vol. *164*, pp 179−191.
(19) Moridis, G. J.; Sloan, E. D. Gas production potential of disperse low-saturation hydrate accumulations in oceanic sediments. *Energy Convers. Manage.* **2007**, *48* (6), 1834–1849.
(20) Su, Z.; Cao, Y.; Wu, N. A model for predicting gas well performance of free gas zone beneath hydrate layer. *J. Pet. Sci. Eng.* **2010**, *71* (3−4), 179–186.
(21) Wu, N. Y.; Zhang, H. Q.; Yang, S. X.; Liang, J. Q.; Wang, H. B. Preliminary Discussion on Natural Gas Hydrate (NGH) Reservoir System of Shenhu Area, North Slope of South China Sea. *Nat. Gas Ind.* **2007**, *27* (9), 1–6.
(22) McDonnell, S. L.; Max, M. D.; Cherkis, N. Z.; Czarnecki, M. F. Tectono-sedimentary controls on the likelihood of gas hydrate occurrence near Taiwan. *Mar. Pet. Geol.* **2000**, *17*, 929–936.
(23) Wu, N. Y.; Zhang, H. Q.; Su, X.; Yang, S. X.; Zhang, G.; Liang, J. Q.; Lu, J.; Gong, J.; Scheltheiss, P.; Holland, M. High concentrations of hydrate in disseminated forms found in very fine-grained sediments of Shenhu area, South China Sea. *Terra Nostra* **2007**, *1−2*, 236–237.
(24) Wu, N. Y.; Yang, S. X.; Zhang, H. Q.; Liang, J. Q.; Wang, H. B.; Su, X.; Fu, S. Y. Preliminary discussion on gas hydrate reservoir system of Shenhu Area, North Slope of South China Sea. In *The 6th International Conference on Gas Hydrate*, Vancouver, British Columbia, Canada, 2008; Paper 5700.
(25) Wu, N. Y.; Yang, S. X.; Zhang, H. Q.; Liang, J. Q.; Wang, H. B.; Lu, J. A. Gas Hydrate System of Shenhu Area, Northern South China Sea:Wire-line Logging, Geochemical Results and Preliminary Resources Estimates. In *Offshore Technology Conference*, Houston, Texas, 2010; Paper 20485.
(26) Zhang, H. Q.; Yang, S. X.; Wu, N. Y.; Scheltheiss, P.; Holland, M.; Zhang, G. X.; Liang, J. Q.; Lu, J., A.; Rose, K. High Concentration Hydrate in Disseminated forms Obtained in Shenhu Area, North Slope of South China Sea. In *The 6th International Conference on Gas Hydrate*, Vancouver, British Columbia, Canada, 2008; Paper 5701.
(27) Schultheiss, P.; Holland, M.; Humphrey, G. Wireline coring and analysis under pressure: Recent use and future developments of the HYACINTH system. *Sci. Drill.* **2009**, *7*, 44–50.

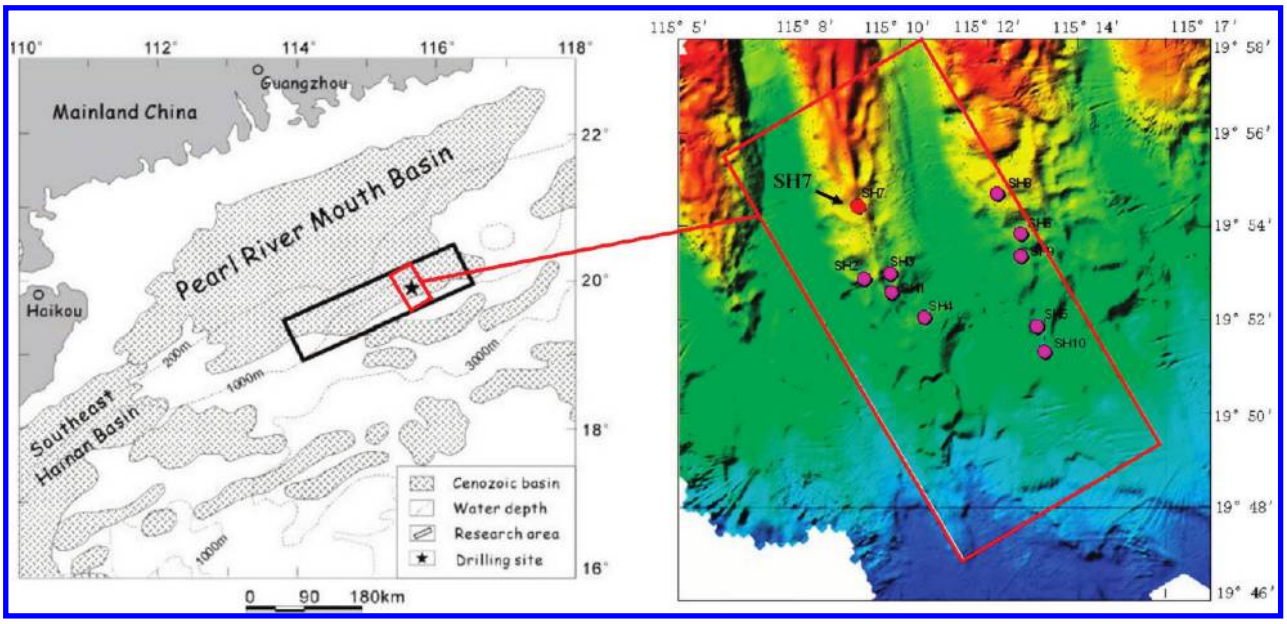

Figure 1. (a) Location of research area, Shenhu Area, north slope of South China Sea and (b) bathymetric map of gas hydrate drilling area with sites drilled in the research area.

Table 1. P-Wave Velocity and Gamma Density of Pressure Cores in Shenhu Area, South China Sea (MSCL-P Logging of Pressure Cores)

sample	depth (mbsf)	gamma density (gm/cm^3)	P-wave velocity (m/s)
SH7B-05P	104	1.85−2.00	1534−1590
SH7B-07R	135	1.83−1.97	
SH7B-11R	155	1.87−2.04	1660−1810
SH7B-15R	163	1.95−2.03	1600−2095
SH7B-23R	185	2.15−2.21	1551−1579

Natural hydrate accumulations are divided into four main classes.[5,11,12] Class 1 accumulations are composed of two layers, including the hydrate-bearing layer (HBL) and an underlying two-phase fluid (containing mobile gas and liquid water) zone. Class 2 deposits include an HBL underlain by a zone of mobile water. Class 3 accumulations involve only an HBL, without underlying mobile fluid zones (and usually bounded by low-permeability overburden and underburden). Class 4 deposits involve disperse low-saturation oceanic hydrate without confining boundaries, which are not likely to have production potential. The hydrate accumulations in the Shenhu Area involve a single HBL within fine-textured sediments and boundaries (overburden and underburden layers) which have the same intrinsic permeabilities with the HBL.

These deposits are considered "challenging" hydrates (CH) for gas production, as they are characterized by the HBL without the confinement of the boundaries, which have the same permeabilities with HBL, type CH-B in the terminology of Moridis et al.,[28] in addition to incidence in fine-textured sediments of low-permeability (type CH-k) such as silts and clays.[21,23−26]

1.4. Objectives. The main objective of this study is the evaluation of the gas production potential of recently discovered marine gas hydrate deposits in the Shenhu Area of the South China Sea, as well as the factors affecting it. Because of the generally low productivity of such challenging oceanic deposits, only horizontal wells are considered in this analysis. Several possible production methods and horizontal well configurations are investigated, and the sensitivity of gas production to various formation and operation parameters and conditions is assessed.

2. System Description and Production Strategies

2.1. Method of Production. Earlier studies[12,14,15] indicated that depressurization is the simplest and most promising hydrate dissociation method, and possibly the only practical option in the majority of hydrate deposits, because of its technical and economic effectiveness. Significant cooling in the vicinity of vertical wellbores (caused by both the endothermic reaction of hydrate dissociation and the Joule−Thompson effect) may induce secondary hydrate formation. This problem, which can lead to flow blockage if left untreated, can be alleviated through the application of thermal stimulation (periodic or continuous, mainly by means of warm water injection), thus enhancing production when used in conjunction with the main dissociation method, i.e., depressurization.[6,11,12] However, pure thermal stimulation appears to be very ineffective as a gas production method when used as the main dissociation strategy.[12]

Constant-pressure production appears to be the most effective method (if not the only option).[12] During the initial stage of production (which constitutes a large part of the entire production period), when the formation effective permeability k_{eff} is very low because of the presence of the solid hydrate, constant-P production allows a continuous increase in the gas production rate Q_{PT}. This is caused by the continuously increasing k_{eff} in the deposit as S_{H} declines in the course of hydrate dissociation. Furthermore, by setting the well pressure $P_{\mathrm{W}} > P_{\mathrm{Q}}$ (i.e., the P at the quadruple point), constant-P production provides the necessary bottomhole pressure control to eliminate the possibility of ice formation and significantly reduce the formation of secondary hydrates.

Despite the well-documented superiority of depressurization-induced dissociation, the low instrinsic permeability k and

(28) Moridis, G. J.; Reagan, M. T.; Boyle, K. L.; Zhang, K. Evaluation of the Gas Production Potential of Challenging Hydrate Deposits. In *TOUGH Symposium*, Lawrence Berkeley National Laboratory, Berkeley, CA, 2009.

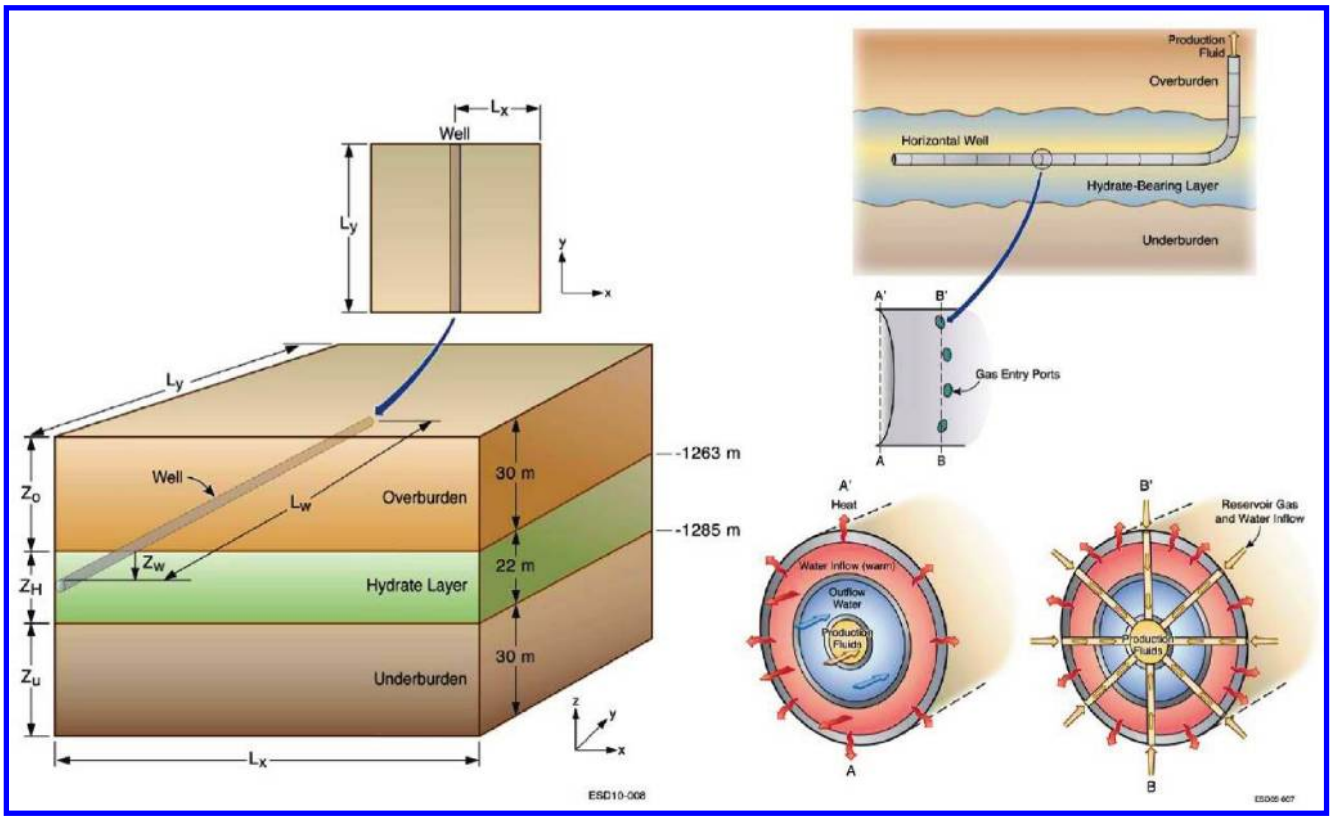

Figure 2. (a) System geometry and configuration of the horizontal well producing from the hydrate deposit at the SH7 site of the Shenhu Area, South China Sea and (b) the new well design for concurrent heat addition and gas production.[24].

the limited confinement effect of the boundaries in the CH-k and CH-B deposits may hinder its application in the Shenhu Area. Aggressive depressurization is inadvisible because it can lead to significant pressure drops in the vicinity of the well, in addition to very large water production. Warm water injection is not recommended because of the limited effectiveness of thermal dissociation methods and of the adverse pressure and relative permeability regime of any gas released from dissociation and attempting to flow toward the well. In this study, production is based on hydrate dissociation induced by a combination of depressurization (the dominant mechanism) and thermal stimulation (in a supporting role), and gas is produced using horizontal wells operating under a constant-pressure regime. The production method attempts to overcome the shortcoming of depressurization and thermal stimulation and is described below.

2.2. Well Design and Description. We consider only horizontal wells (Figure 2) in this study because earlier studies[13,29,30] showed that the performance of horizontal wells is superior to that of vertical wells in gas production, one of the reasons being that they virtually eliminate the problem of secondary hydrate formation. We evaluate the performance of a single horizontal well of $r_W = 0.1$ m placed in the middle of the 22 m-thick HBL (Figures 2a and 3a) at the SH7 site of the Shenhu Area.

We use the new well design proposed by Moridis et al.,[28] which combines a mild constant-P depressurization regime with a thermal stimulation process that provides heat to the HBL by means of warm water (originating from deeper, warmer reservoirs) circulating inside the wellbore without injection into the deposit (Figure 2b). The higher T around the well is expected to promote hydrate dissociation, in addition to preventing the formation of secondary hydrates around the wellbore. The mild depressurization regime of this well design is designed to prevent excessive water production, and the constant-P production regime eliminates the possibility of excessive pressure drops. The continuous addition of heat without resorting to warm water injection into the HBL does not negate (even partially) the effects of depressurization, does not further burden the relative permeability regime of the gas evolving from dissociation, and does not inhibit flow to the well.

3. Numerical Models and Simulation Approach

3.1. Numerical Simulation Code. For this numerical simulation study, we used both the serial and parallel versions of the TOUGH+HYDRATE code.[31,32] This code can model nonisothermal hydration reactions, phase behavior, and flow of fluids and heat under the conditions typical of natural CH_4-hydrate deposits in complex geologic media. It includes both an equilibrium and a kinetic model of hydrate formation

(29) Reagan, M. T.; Boyle, K. L.; Zhang, K. Sensitivity Analysis of Gas Production from Class 2 and Class 3 Hydrate Deposits. In *Offshore Technology Conference*, Houston, Texas, 2008; Paper 19554.

(30) Rutqvist, J.; Moridis, G. J. Numerical Studies on the Geomechanical Stability of Hydrate-Bearing Sediments. *SPE J.* **2009**, *14* (2), 267–282.

(31) Moridis, G. J.; Kowalsky, M. B.; Pruess, K. *TOUGH+HYDRATE v1.1 User's Manual: A Code for the Simulation of System Behavior in Hydrate-Bearing Geologic Media*; Lawrence Berkeley National Laboratory: Berkeley, CA, 2009.

(32) Zhang, K.; Moridis, G. J.; Wu, Y. S.; Pruess, K. A Domain Decomposition Approach for Large-Scale Simulations of Flow Processes in Hydrate-Bearing Geologic Media. In *The 6th International Conference on Gas Hydrate*, Vancouver, British Columbia, Canada, 2008; Paper 5480.

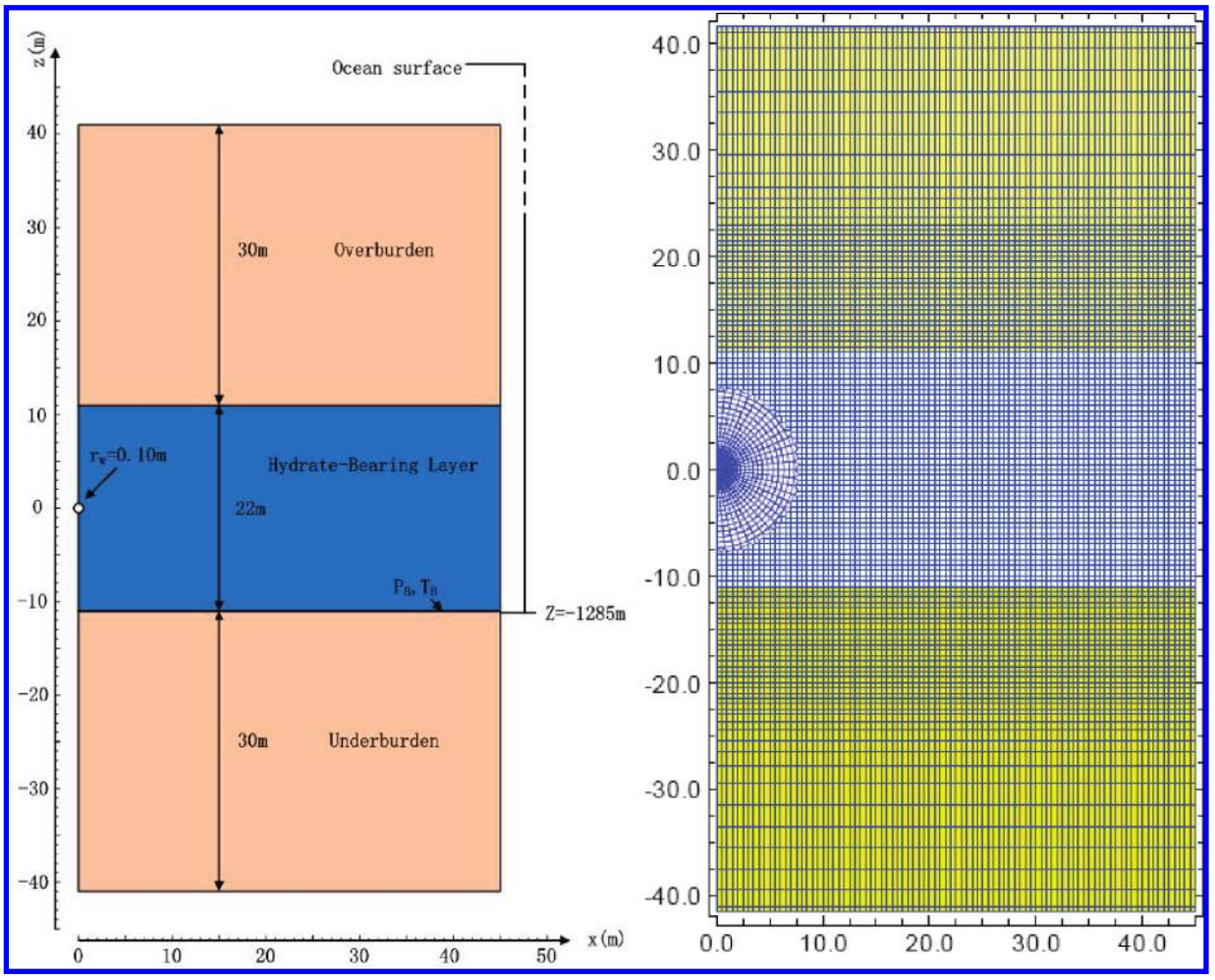

Figure 3. (a) Schematic of the marine hydrate deposit at the SH7 site of the Shenhu Area, South China Sea and (b) grid used in the simulations.

and dissociation. The model accounts for heat and up to four mass components (i.e., water, CH_4, hydrate, and water-soluble inhibitors such as salts or alcohols) that are partitioned among four possible phases: gas, aqueous liquid, ice, and hydrate. A total of 15 states (phase combinations) can be described by the code, which can handle any combination of hydrate dissociation mechanisms and can describe the phase changes and steep solution surfaces typical of hydrate problems. In this code, the impact of the movement and the volume expansion of the sediments are neglected.

3.2. Geometry, Domain Discretization, and System Properties. The geologic system in this study corresponds to the site SH7 at the Shenhu Area. Analysis of hydrate sample from this site indicated almost pure (99.2%) CH_4-hydrate in clayey sediments. The system properties and initial conditions that were used in the simulations are shown in Table 2. In the absence of direct measurements of the flow properties of the porous media at the site, the estimates of k, ϕ, and the wettability properties (capillary pressure and relative permeabilities, with all related parameters) in Table 2 were based on the similarity of these fine media (silts and clays) to similarly textured soils with known properties. The wellbore was simulated as a pseudoporous medium with $\phi = 1.0$, $k = 5.0 \times 10^{-9}$ m^2 (5000 darcys), a capillary pressure $P_{cap} = 0$, and aqueous and gas relative permeabilites (k_{rA} and k_{rG}) as linear functions of the aqueous and gas phase saturations (S_A and S_G), respectively.

The seafloor at this site is at 1108 m depth, and the HBL extends from 155 to 177 m interval below the seafloor (22 m thick). As in all simulations of this kind, the domain includes an additional 30 m of underburden and overburden (having the same flow properties as the HBL), above and below which boundaries of constant conditions (P and T) are imposed. The 30 m-thickness was shown to be sufficiently large for an accurate description of (a) the heat flow regime through the overburden and underburden during a maximum of 30 years of production[5,11,12] and (b) of the pressure and flow regime, given the low k and the mild depressurization regime.

The geometry and configuration of the hydrate deposit, as well as the corresponding simulation grid, are shown in Figure 3. Because of the limited confinement effect of the boundaries above the HBL and the tendency of gas from hydrate dissociation to accumulate at the top of the formation where an upper dissociation interface develops,[11,12,14,30] the well is placed at the center of the HBL (rather than at the top), i.e., at $x = 0$ and $z = 0$ in the coordinates of the grid in Figure 3b. Because of symmetry about the well, only half of the domain ($x \geq 0$) is simulated. Assuming uniformity of behavior along the length of the horizontal well (i.e., ignoring possible heel to toe deviations in behavior), only a single unit of length $\Delta y = 1$ m needed to be simulated. A no-flow boundary (i.e., no fluid flow and heat transfer) is applied at $x = 45$ m, indicating a well spacing of 90 m. A 1000 m-long well is assumed in all cases.

Table 2. Properties and Conditions of the Hydrate Deposit at Site SH7 in Shenhu Area, South China Sea

parameter	value
overburden thickness ΔZ_O	30 m
HBL thickness ΔZ_H	20 m
underburden thickness ΔZ_U	30 m
well position above the HBL base ΔZ_W	11 m
initial pressure P_B (at base of HBL)	13.83 MPa
initial temperature T_B (at base of HBL)	287.31 K (14.15 °C)
initial saturation in the HBL	$S_H = 0.44$, $S_A = 0.56$
gas composition	100% CH_4
geothermal gradient	0.0433 K/m
water salinity (mass fraction)	0.0305
intrinsic permeability $k_x = k_y = k_z$ (all formations)	7.5×10^{-14} m^2 (= 75 mD)
porosity ϕ (all formations)	0.41
grain density ρ_R (all formations)	2600 kg/m^3
dry thermal conductivity $k_{\Theta RD}$ (all formations)	1.0 W/m/K
wet thermal conductivity $k_{\Theta RW}$ (all formations)	3.1 W/m/K
composite thermal conductivity model[31,34]	$k_{\Theta C} = k_{\Theta RD} + (S_A^{1/2} + S_H^{1/2})(k_{\Theta RW} - k_{\Theta RD}) + \phi S_I k_{\Theta I}$
capillary pressure model[35]	$P_{cap} = -P_{01}[(S^*)^{-1/\lambda} - 1]^{1-\lambda}$
	$S^* = (S_A - S_{irA})/(1 - S_{irA})$
S_{irA}	0.29
λ	0.45
P_{CO}	10^5 Pa
relative permeability model[31]	$k_{rA} = (S_A^*)^n$
	$k_{rG} = (S_G^*)n^G$
	$S_A^* = (S_A - S_{irA})/(1 - S_{irA})$
	$S_G^* = (S_G - S_{irG})/(1 - S_{irA})$
	original porous medium (OPM)
n	3.572
n_G	3.572
S_{irG}	0.05
S_{irA}	0.30

The hybrid grid in Figure 3b comprises 11 259 nonuniformly sized elements, of which 11 034 are active (the remaining being boundary cells). The uppermost and lowermost layers, which are inactive boundary cells, correspond to the constant-P and T conditions discussed earlier. Because of the importance of a high definition in the vicinity of the wellbore, a very fine discretization is used (with gridblocks smaller than 0.1 m across) in the region defined by the center of the well and for $r < 7.5$ m (Figure 3b). Outside this region, $\Delta x = 0.5$ m, but discretization along the z-axis is generally nonuniform. It is fine ($\Delta z \leq 0.5$ m) in the HBL, at the bottom of the overburden, and at the top of the underburden, but it becomes coarser for $z > 22$ m and for $z < -22$ m. Such fine discretization is necessary to correctly describe the spatial distributions of important properties and conditions in the domain and to yield accurate predictions of production.[5,11] Assuming an equilibrium reaction of hydrate dissociation,[31,33] this grid results in 44 136 coupled equations that are solved simultaneously.

3.3. Initial Conditions. The geothermal gradient was estimated from *in situ* measurements:[21] the temperatures of the sample SH7B-FPWS1 (137 mbsf), SH7B-FPWS2 (180 mbsf), and SH7B-FPWS3 (196 mbsf) at site SH7 were 12.49, 14.39, and 15.04 °C, respectively. From these T-measurements and the known T_{OF}, the local (average) geothermal gradient at the SH7 site was computed as $dT/dz = 0.0432$ °C/m and was used to obtain T-estimates at the constant-condition boundaries (upper and lower) of the domain.

With the use of the system geometry (Figure 2a), all the T-related information, the known density of the ocean water as a function of P, T, and salt concentration (1035 kg/m^3 at T_{OF} and atmospheric pressure), the known phase saturation distributions ($S_H = 0.44$ and $S_A = 0.56$ in the HBL; $S_H = 0$ and $S_A = 1$ in both the overburden and the underburden), and the general rule that the pressure distribution in hydrate systems follows the hydrostatic gradient,[11,12] the P- and T-distribution of the initial P- and T-distribution presupposed knowledge of the formation (a) porosity ϕ and (b) wet and dry thermal conductivity, $k_{\Theta Rw}$ and $k_{\Theta RD}$, respectively; the former was determined from *in situ* measurements,[21,23−25] and reasonable estimates were used for the latter (Table 2). The initial P at the HBL bottom ($z = -1285$ m) was estimated as $P_B = 13.83$ MPa (Figures 2a and 3a; Table 2), which is close to the equilibrium hydrate pressure at the temperature $T_B = 14.15$ °C of the HBL base and for $X_S = 0.0305$.

The thermodynamic desirability of hydrate deposits as gas production targets increases with the proximity of P_B to the equilibrium pressure at T_B because such systems are easy to destabilize with mild depressurization or thermal stimulation. The gas hydrate accumulation at the SH7 site of the Shenhu Area appears to be such a thermodynamically appealing target, but this thermodynamic attractiveness is only one of the factors, insufficient by itself, that determines the overall production potential of a deposit.

4. Production from Site SH7 in Shenhu Area: The Reference Case

4.1. Reference Case. The properties and conditions pertaining to the reference case are listed in Table 2. The temperature of the circulating hot water in the well $T_W = 14$ °C, i.e., roughly equal to the initial temperature T_B at the base of the HBL and very slightly warmer than the initial temperature at the elevation of the horizontal well (= 13.7 °C). Such a low T_W effects minimal thermally induced dissociation of hydrates in the HBL that can only begin once P has dropped below the equilibrium pressure corresponding to

(33) Kowalsky, M. B.; Moridis, G. J. Comparison of kinetic and equilibrium reaction models in simulating gas hydrate behavior in porous media. *Energy Convers. Manage.* **2007**, *48* (6), 1850–1863.

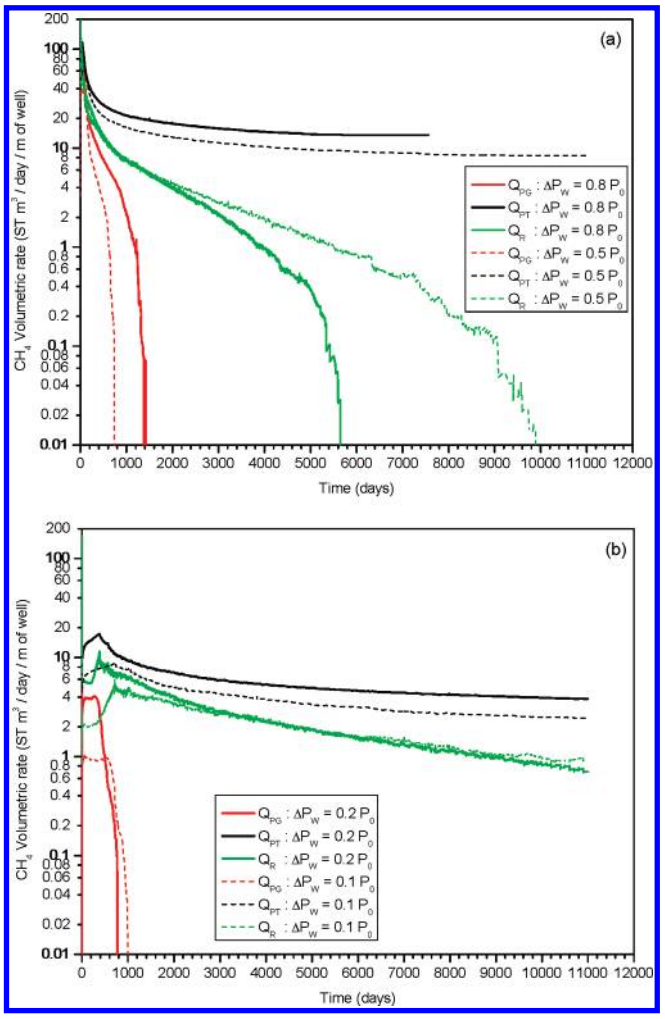

Figure 4. Volumetric rate of CH_4 production in the gas phase (Q_{PG}), the total gas production (Q_{PT}) at the well and released from hydrate dissociation (Q_R) using the depressurization method with $\Delta P_W = 0.8P_0$, $0.5P_0$, $0.2P_0$, and $0.1P_0$, $T_0 = 13.7$ °C during gas production from the methane hydrate deposit in this study.

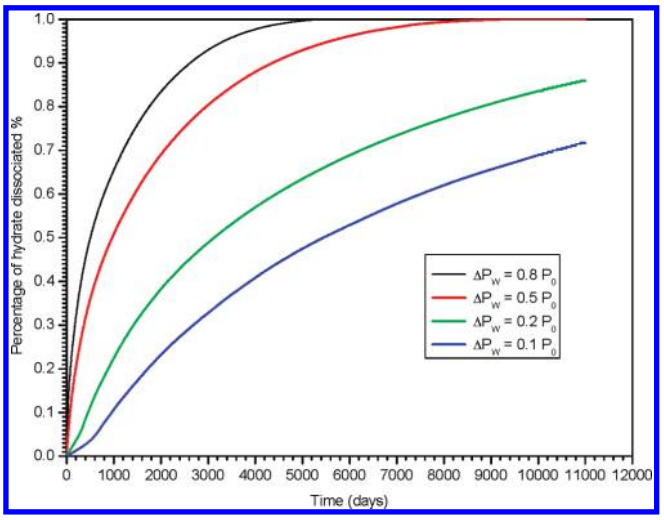

Figure 5. Percentage of hydrate dissociated % using the depressurization method with $\Delta P_W = 0.8P_0$, $0.5P_0$, $0.2P_0$, and $0.1P_0$, $T_0 = 13.7$ °C during gas production from the methane hydrate deposit in this study.

T_W. The driving force of the depressurization process $\Delta P_W = P_0 - P_W = 0.8P_0$, $0.5P_0$, $0.2P_0$, and $0.1P_0$, where PW is the constant bottomhole pressure at which the well operates and $P_0 = 13.7$ MPa is the initial P in the HBL at the elevation of the production well. The $\Delta P_W = 0.2P_0$ case is treated as the base case in this study. Of the ΔP_W levels explored here, $0.2P_0$ (base case) and $0.1P_0$ are routinely attained in field operations, $0.5P_0$ represents the outer envelope of field application, and $0.8P_0$ is an extreme case of depressurization.

4.2. Gas and Water Production. Figure 4 shows the evolution of the volumetric rate of CH_4 production in the gas phase (Q_{PG}), the total gas production (Q_{PT}) at the well, and the gas released from hydrate dissociation (Q_R). The difference $Q_{PD} = Q_{PT} - Q_{PG}$ describes the produced gas that is dissolved in the produced aqueous phase. Note that Q_{PT} exceeds Q_R in all the different ΔP_W cases and that Q_{PG} is much smaller than Q_{PT}, which means that the source of the majority of the produced gas is CH_4 dissolved in the water, rather than from the free gas phase. Figure 5 shows the percentage of hydrate dissociated in the entire simulated domain. As shown in Figure 4a, Q_R decreases to a very low level ($Q_R < 0.01$ ST m^3/day/m of well) at $t = 5600$ and 10 000 days in $\Delta P_W = 0.8P_0$ and $0.5P_0$ cases, respectively; the corresponding hydrate dissociation percentage shown in Figure 5 approaches 1.0, which indicates that almost all the hydrate in the deposit disappears at that time. In the $\Delta P_W = 0.2P_0$ and $0.1P_0$ cases, there are still hydrates in the deposit at the end of the production periods ($t = 30$ years).

A local maximum of $Q_{PT} = 17.3$ ST m^3/day/m of the well is reached before a decline begins at about $t = 390$ days in the $\Delta P_W = 0.2P_0$ case (Figure 4b). The Q_{PTmax} for the entire deposit reaches 3.46×10^4 ST m^3/day (1.22 MMSCFD). Meanwhile, the corresponding Q_R shows the similar profile as Q_{PT} as shown in Figure 4b.

This is attributed to a combination of (a) an increase in the effective permeability in the vicinity of the well at early times of the production process (approximately $t = 0-390$ days) because of the hydrate dissociation on this area under the constant driving force of depressurization; (b) the breakthrough of the water from the underburden (Figure 10), which provides another source of water to reduce the effect of depressurization on gas production at the well; (c) some gas may escape from the dissociated zone in the deposit (in the initial HBL) to the ocean through overburden because of buoyancy, especially after the water breakthrough from the overburden to the cylindrical dissociated zone around the well; (d) the resulting lower T, which further slows dissociation after 390 days.

Figure 6 shows the corresponding water production rates Q_W and gas-to-water ratios $R_{GW} = V_P/M_W$, where V_P is the cumulative volume of the produced CH_4, and M_W is the cumulative mass of the produced water. R_{GW} provides a measure of the hydrate system response and the effectiveness of dissociation as a gas-producing method. In $\Delta P_W = 0.2P_0$ case, Q_W over 6000 kg/day/m of well is reached after approximately $t = 1100$ days. The water production rate is $Q_W = 1.2 \times 10^7$ kg/day (1.2×10^4 ton/D), which is unmanageable, and R_{GW} is prohibitively low ($R_{GW} < 5$ ST m^3 of CH_4/m^3 of H_2O/m of well). A higher ΔP_W (the driving force of depressurization) appears to have a remarkable effect on gas production,

(34) Moridis, G. J.; Seol, Y.; Kneafsey, T. J. Studies of reaction kinetics of methane hydrate dissociation in porous media. In *The 5th International Conference on Gas Hydrate*, Trondheim, Norway, 2005; Paper 1004.

(35) van Genuchten, M. T. A Closed-Form Equation for Predicting the Hydraulic Conductivity of Unsaturated soils. *Soil Sci. Soc. Am. J.* **1980**, *44*, 892–898.

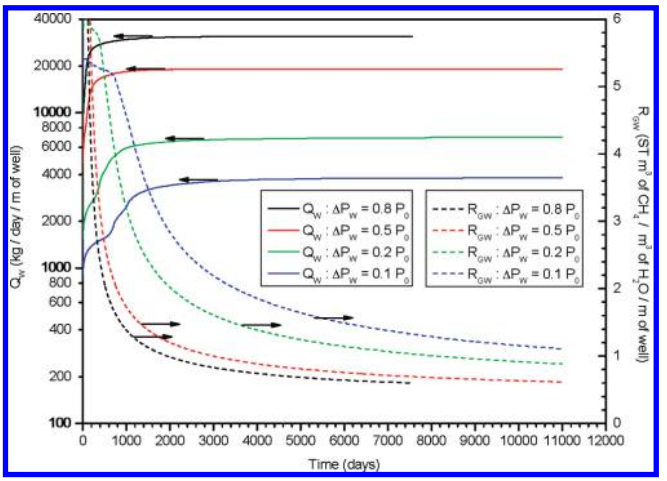

Figure 6. Evolution Q_W and R_{GW} using the depressurization method with $\Delta P_W = 0.8P_0$, $0.5P_0$, $0.2P_0$, and $0.1P_0$, $T_0 = 13.7$ °C during gas production from the methane hydrate deposit in this study.

long-term $Q_{PT} < 20$ ST m^3/day/m of well in the $\Delta P_W = 0.2P_0$ case (Figure 4), while for the $\Delta P_W = 0.8P_0$ case, long-term $Q_{PT} < 4.00 \times 10^4$ ST m^3/day (1.41 MMSCFD) and about 7 times lower than the rule-of-thumb for commercially viable production rates from offshore gas wells.

4.3. Spatial Distribution of S_H and S_G. Figures 7−11 show the evolution of the S_H, S_G, T, and X_S distributions over time in the HBL ($-11 < z < 11$) using the depressurization method for gas production, with $\Delta P_W = 0.2P_0$ and $T_0 = 13.7$ °C, while Figure 9 shows the evolution of the P distribution over time in the entire deposit ($-41 < z < 41$, see Figure 3a). Comparison of the hydrate spatial distribution over 30 years to the initial HBL provides a measure of the hydrate dissociation profile.

Figures 7 and 8 show the evolution of the S_H and S_G spatial distribution over time in the HBL. The figures show (i) the initial hydrate dissociation around the well, with limited cylindrical dissociation interface; (ii) the evolution of the upper and the lower dissociation interface; (iii) the mergence of the lower dissociation interface and the cylindrical

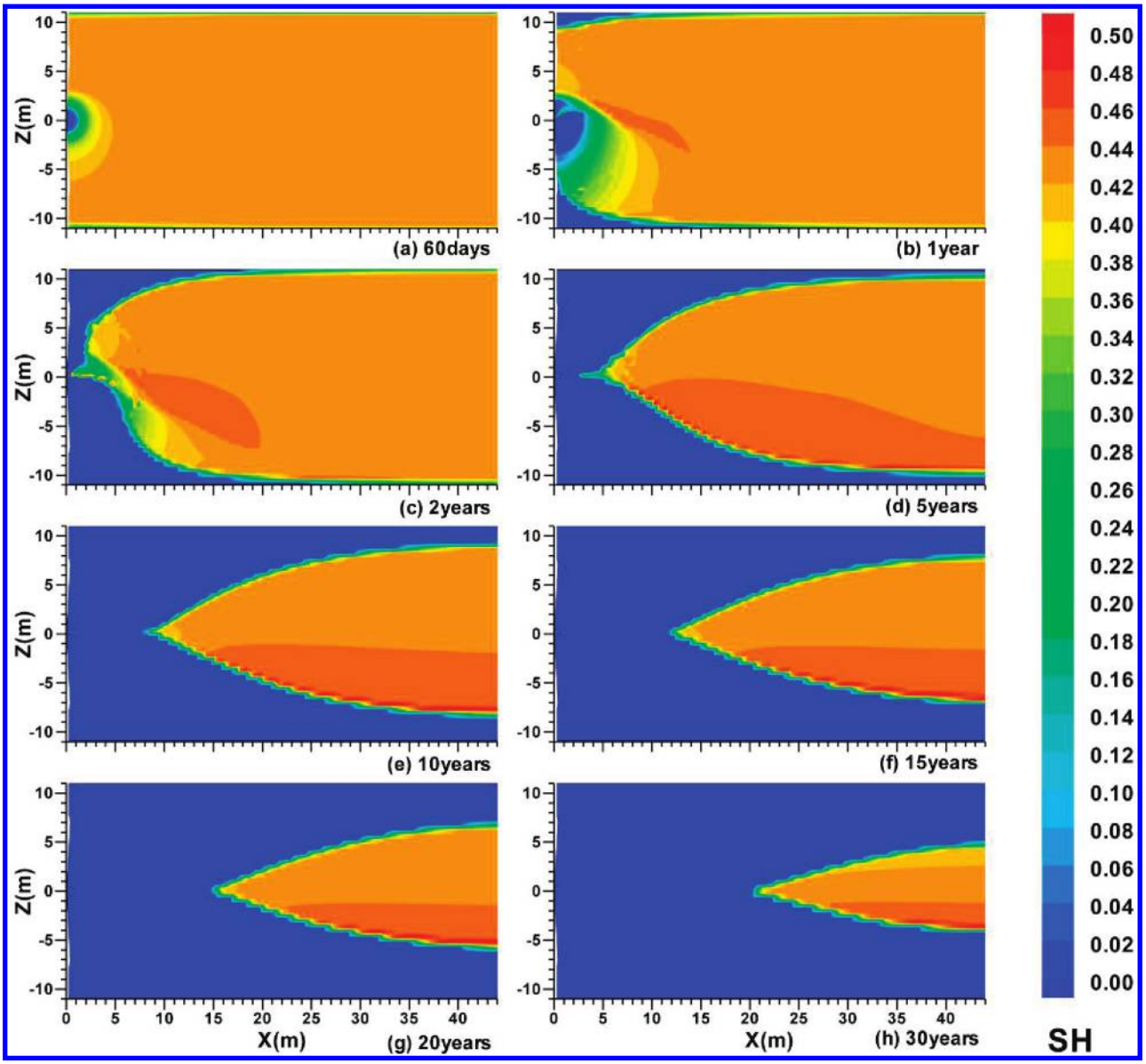

Figure 7. Evolution of spatial distribution of S_H when $\Delta P_W = 0.2P_0$ during gas production from the methane hydrate deposit at the SH7 Site of the Shenhu Area, South China Sea.

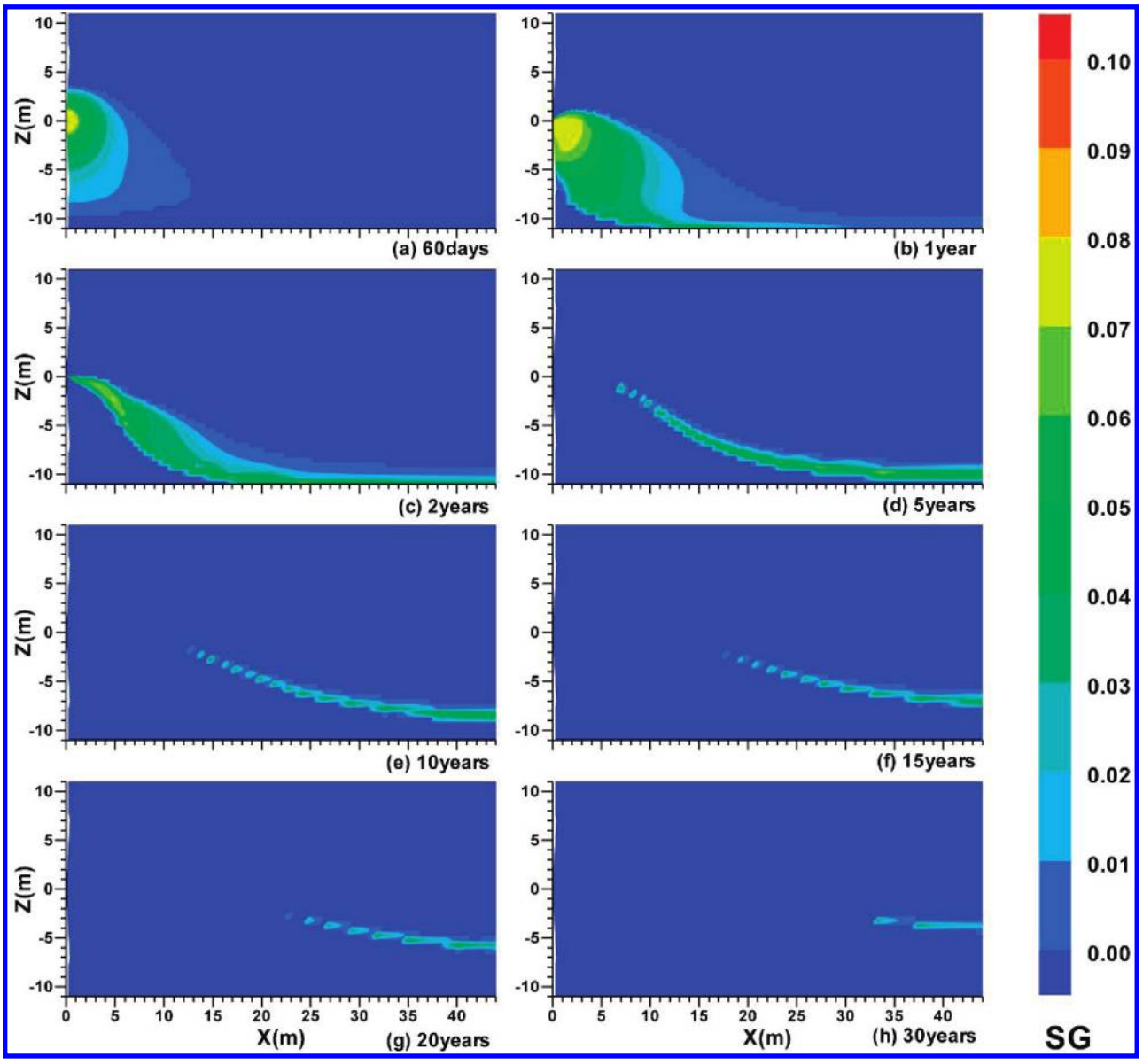

Figure 8. Evolution of spatial distribution of S_G when $\Delta P_W = 0.2P_0$ during gas production from the methane hydrate deposit at the SH7 Site of the Shenhu Area, South China Sea.

interface around the well, which happens earlier than that of the upper and cylindrical interfaces; (iv) the evolution of the high-S_H region (secondary hydrate formation) immediately above the lower dissociation front; (v) limited secondary hydrate formation near the well; (vi) the accumulation of gas around the well within the cylindrical dissociated zone at early times and then below the lower dissociation interface at later times. Of those, (i) and (ii) are results of the continuing pressure drop and the low effective permeability k_{eff} of the HBL in the area surrounding the dissociated zone; (ii) and (iii) are caused by the heat and fluid flow from both the upper and lower boundaries (overburden and underburden), especially the effect of the relatively warmer fluid from the underburden (Figure 10), (iv) occurs because the fluids (gas and water) released from the hydrate dissociation on the lower dissociation front move both toward the well and deeper into the hydrate body (away from the well), which causes secondary hydrate formation and higher S_H than initially, and (v) is the result of the constant-pressure production under the reasonable driving force ($\Delta P_W = 0.2P_0$).

A comparison with the cases involving an impermeable upper boundary[15] where a maximum of $S_G > 0.5$ is attained along the bottom of the overburden, there is no such upper permeability barrier here, and the S_G in the deposit is much lower, with a maximum of S_G of about 0.10. The S_G distributions in Figure 8a,b indicate gas accumulation in the cylindrical dissociated zone around the well, leading to the highest S_G observed in the deposit. The reason for this gas accumulation is the continuing dissociation along the cylindrical interface around the well, in addition to the rising of the gas released from below the wellbore. This gas accumulation continues until breakthrough occurs, caused by the hydrate dissociation between the wellbore and the top of the HBL, which connects the overburden to the cylindrical zone around the well, (the undissociated HBL with low k_{eff} plays an important role as a barrier to upward movement that leads to gas accumulation). Some of the gas released along the upper interface does not accumulate in the deposit due to the permeability of the overburden. As already discussed in the case of $\Delta P_W = 0.2P_0$ in Figure 4b, the Q_{PG} is much smaller

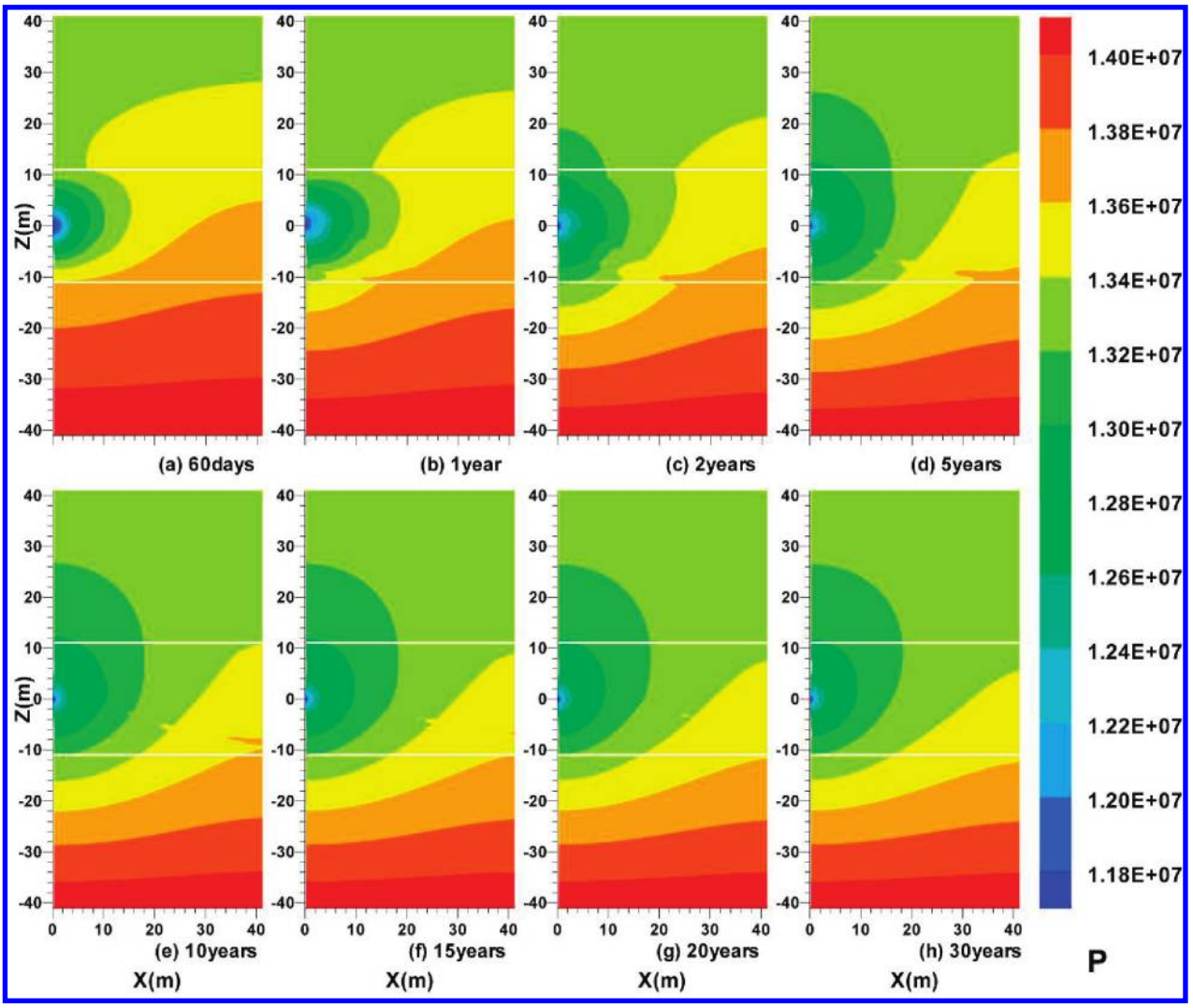

Figure 9. Evolution of spatial distribution of P when $\Delta P_W = 0.2P_0$ during gas production from the methane hydrate deposit at the SH7 Site of the Shenhu Area, South China Sea.

than Q_{PT} and decreases rapidly to a very low level (less than 0.01 ST m^3/day/m of well) from about $t = 270-800$ days, which means there is little methane produced in the gas phase. The S_G distribution over 2 years in Figure 8 (Figure 8c and beyond) validate the hypothesis that the disappearance of the upper barrier and the upper water breakthrough lead to gas losses through the overburden toward the surface, with undesirable consequences, such as low Q_{PT} (Figure 4b) and low R_{GW} (Figure 6), if such releases cannot be contained.[14,15] The small gas accumulation (with local $S_G < 0.1$) immediately below the lower dissociation interface could not be produced as gas phase from the well and rises toward the overburden over 2 years.

The emergence of the lower dissociation interface and the cylindrical interface around the well at about 1 year in Figure 7 is remarkable. As already discussed in the case of $\Delta P_W = 0.2P_0$ in Figure 4b, the Q_{PT} declines monotonically after about $t = 390$ days because of the water breakthrough from the underburden to the cylindrical dissociated zone around the well (in other words, the lower dissociation interface and the cylindrical interface have merged) that causes the promotion of water (rather than gas) production and alleviation of the effect of depressurization on gas production at the well. This water flow from the underburden to the well affects the S_G distribution around the well (especially evident in Figure 8c and beyond). Although there is cooling effect caused by the endothermic hydrate dissociation, the temperature in the HBL at $t = 1$ year is even higher than that in the initial HBL (Figure 10), which validate the hypothesis of water flow from the underburden.

4.4. Spatial Distribution of *P*. Figure 9 shows the evolution of the P distribution over time within the entire deposit ($-41 < z < 41$), with $\Delta P_W = 0.2P_0$ and $T_0 = 13.7$ °C during gas production. White lines in Figure 9 indicate the initial position of the top and base of the HBL at $z = 11$ and $z = -11$, respectively (Figure 3a). Figure 9 shows (i) the evolution of the pressure gradient around the well over time; (ii) the pressure drop in the overburden and underburden; (iii) the jagged P distribution and the inflections near the interface of the dissociated and undissociated zone in the HBL. Of those, (i) and (ii) result from the characteristic of the permeabilities of boundaries, and (iii) results from fluid flow caused by gas and water dissociated from the hydrate.

Figure 9a,b shows a confined cylindrical zone, corresponding to the dissociated zone shown in Figure 7a,b, with pressure gradients oriented toward the well. The constant pressure in the well with $\Delta P_W = 0.2P_0$ is about $P_W = 11.2$ MPa. The radius of the cylindrical low-pressure zone

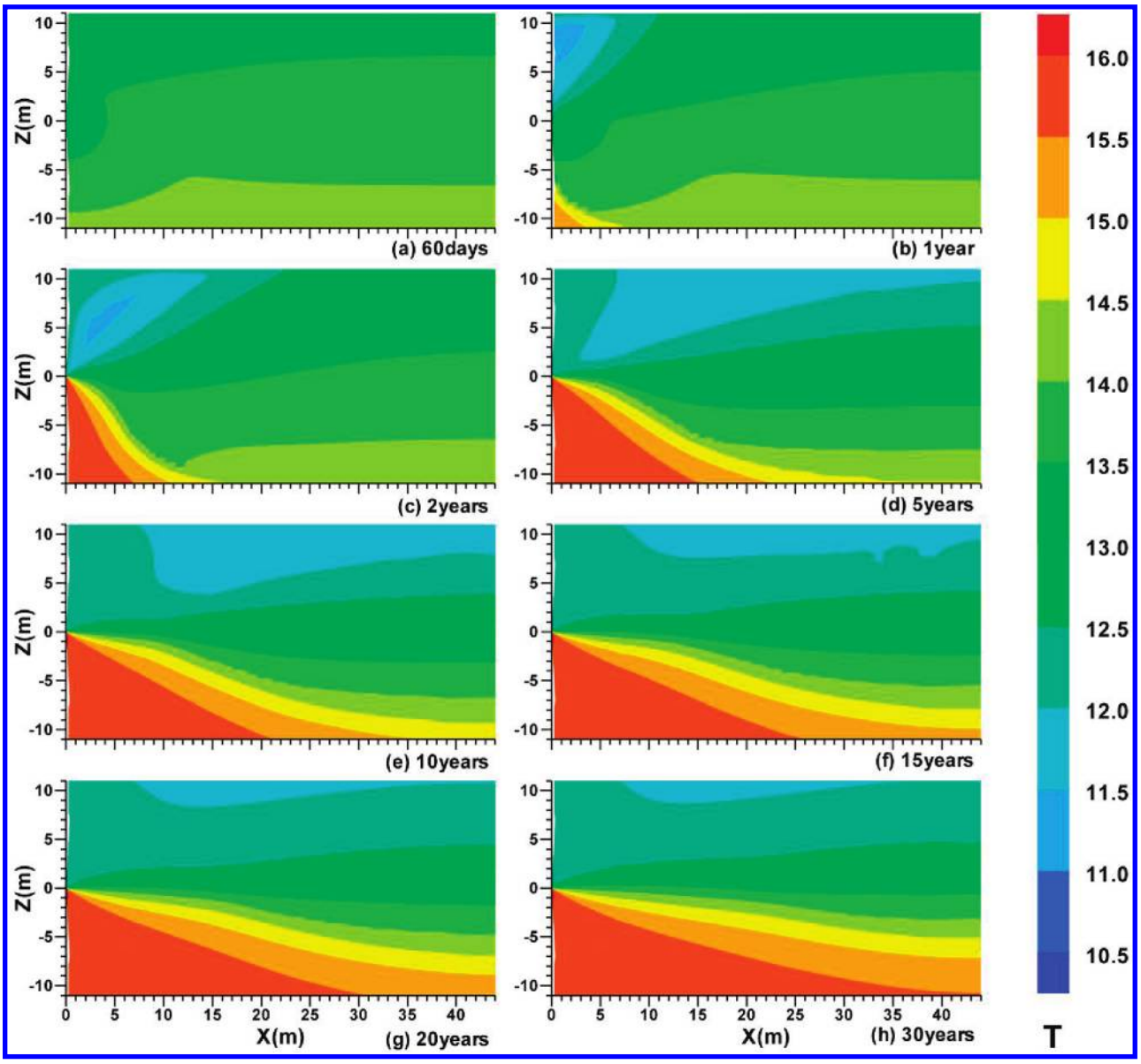

Figure 10. Evolution of spatial distribution of T when $\Delta P_W = 0.2P_0$ during gas production from the methane hydrate deposit at the SH7 Site of the Shenhu Area, South China Sea.

(defined as the zone with pressure lower than 12.5 MPa) around the well is larger than 2 m as shown in Figure 9a,b. As the pressure in the well P_W remains constant during the entire production process, the pressure gradients and spatial distributions are affected by the hydrate dissociation and the corresponding fluid flow patterns. The cylindrical zone around the well could be more effectively depressurized, owing to the low effective permeability k_{eff} of the HBL in the area surrounding the dissociated zone (cylindrical low-pressure zone). In Figure 9c−h, as the water breaks through from the underburden and overburden to the dissociated zone around the well, the radius of the cylindrical low-pressure zone around the well decreases to approximately 1 m.

The pressures in the overburden and underburden drop significantly because of fluid flow toward the production well. As shown in Figure 9a−d, in the first 5 years, the pressures in the overburden and underburden drop significantly over time, while the P distribution in the overburden and underburden changes only slightly from 10 to 30 years (Figure 9e and beyond). The reason for this is that after 10 years, hydrate distribution in the HBL has a limited effect on the fluid flow in the system, and the pressure distribution becomes practically stable.

In Figure 9a−d, there are inflections in the P contours at the top white line indicating the initial position of the top HBL at $z = 11$. Also, in Figure 9b−f, obvious jagged P distributions are shown near (especially above) the lower white line, which indicate the initial position of the base of the HBL at $z = -11$. All the inflections and jagged positions shown in Figure 9 correspond to the interface of the dissociated and undissociated zone in the HBL shown in Figure 7.

4.5. Spatial Distribution of *T*. Figure 10 shows the evolution of the T distribution over time in the HBL when $\Delta P_W = 0.2P_0$ during production. The low-T zone (defined as the zone with $T < 11.5$ °C) in Figure 10b,c occurs in the vicinity of the upper dissociation interface (Figure 7b,c), which indicates cooling as dissociation and production proceed. The low-T zone disappears in Figure 10d and beyond because of encroachment by warmer water flowing from the overburden (where there is an inversion of the geothermal gradient,

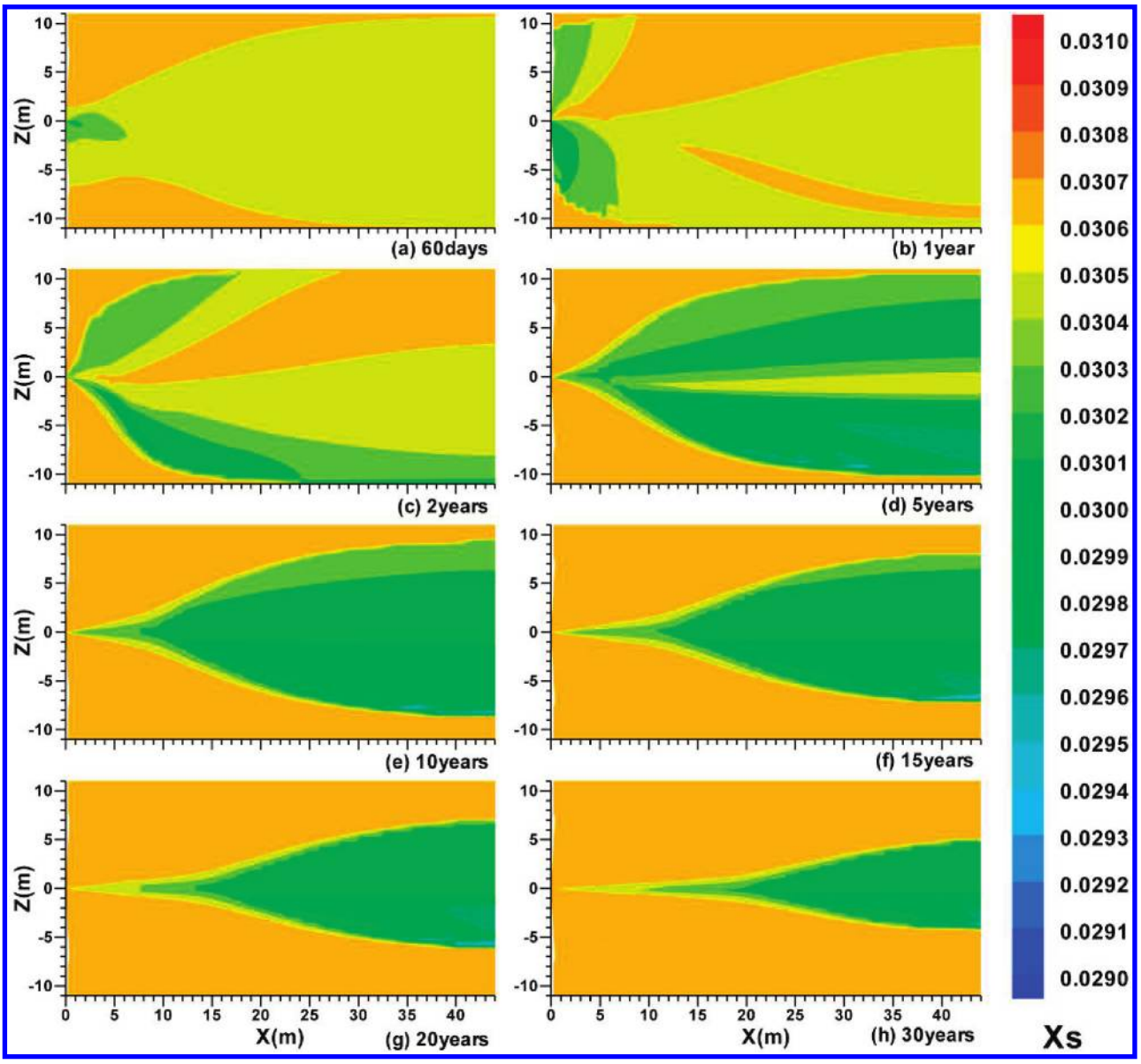

Figure 11. Evolution of spatial distribution of X_S when $\Delta P_W = 0.2P_0$ during gas production from the methane hydrate deposit at the SH7 Site of the Shenhu Area, South China Sea.

as a result of dissociation-induced cooling in the HBL). The warmer water rising from the underburden is clearly depicted by the spatial distribution of T in the vicinity of the lower dissociation interface (Figure 7). All fluids of different origin and temperature, including the original free water in the HBL, the gas and water produced from hydrate dissociation, the water from the overburden, and the warmer water rising from the underburden, converge toward the well.

4.6. Spatial Distribution of X_S. Figure 11 shows the distribution of the salt concentration (expressed as the mass fraction of salt X_S in the aqueous phase) over time in the HBL ($-11 < z < 11$) using the depressurization method, with $\Delta P_W = 0.2P_0$ and $T_0 = 13.7$ °C during gas production from methane hydrate deposit in this work. The dilution effect of dissociation on salinity is clearly shown in Figure 11. Because the salts cannot be included in the hydrate crystals, fresh water is released from hydrate dissociation and reduces the water salinity *in situ*. Thus, the locations of intense dissociation activity can be identified as the loci of low salinity.[15] Unlike the cases with impermeable boundaries, which means the limited replenishment of salinity from water flowing from nearly impermeable boundaries,[15] the salinity distributions in Figure 11 are significantly affected by the water flow from the overburden and underburden.

In Figure 11a,b, the maximum X_S reduction is observed near the well, corresponding to the cylindrical dissociated zone in Figure 7 and the low T zone in Figure 10, which is affected by the water flow from the overburden. In Figure 11c and beyond, the spatial distribution and shapes of the X_S reduction areas are similar to the undissociated zone shown in Figure 7 and reflect the continuous flow of saline water from the boundaries, along the dissociation hydrate boundary, and to the well.

5. Sensitivity analysis of production from site SH7 of the Shenhu Area

In this work, we investigated the sensitivity of gas production to the following conditions and parameters: the initial hydrate saturation S_{H0}, the intrinsic permeability k, the temperature

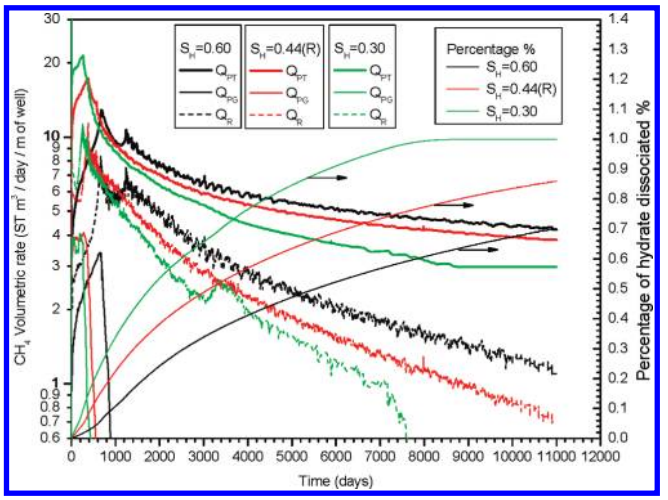

Figure 12. Sensitivity analysis: effect of S_{H0} on Q_{PG}, Q_{PT}, Q_R and the percentage of hydrate dissociated when $\Delta P_W = 0.2P_0$ during gas production from the methane hydrate deposit at the SH7 Site of the Shenhu Area, South China Sea ($S_{H0} = 0.44$ in the reference case).

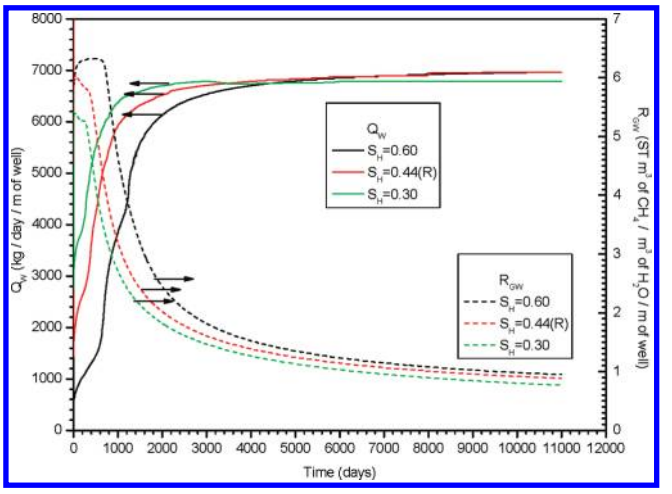

Figure 13. Sensitivity analysis: effect of S_{H0} on the evolution Q_W and R_{GW} when $\Delta P_W = 0.2P_0$ during gas production from the methane hydrate deposit at the SH7 Site of the Shenhu Area, South China Sea ($S_{H0} = 0.44$ in the reference case).

of the circulating hot water in the well T_W, and the initial temperature T_0.

5.1. Sensitivity to S_{H0}. Figures 12 and 13 show, respectively, the dependences of (a) Q_{PG}, Q_{PT}, Q_R, and the percentage of hydrate dissociated in the HBL and (b) Q_W and R_{GW} on the initial hydrate saturation S_{H0}. For the reference case, $S_{H0} = 0.44$, which is already discussed above.

As already shown in Figure 4, a local maximum of $Q_{PT} = 17.3$ ST m^3/day/m of well is reached before a decline begins at about $t = 390$ days, for the $\Delta P_W = 0.2P_0$ case with the initial hydrate saturation $S_{H0} = 0.44$ (reference case). As shown in Figure 12, the maximum of $Q_{PT} = 21.5$ ST m^3/day/m of well is reached at about $t = 265$ days when $S_{H0} = 0.30$, while the maximum of $Q_{PT} = 13.0$ ST m^3/day/m of well is reached at about $t = 680$ days when $S_{H0} = 0.60$. A lower S_{H0} leads to a higher maximum of Q_{PT} reached much earlier than the higher S_{H0} cases. The reason for this is that the higher initial k_{eff} in the lower S_{H0} cases leads to a faster depressurization and hydrate dissociation earlier in the production process.

After reaching the maximum, a decline of Q_{PT} begins, which lasts to the end of the simulation, and a lower S_{H0} leads to a lower Q_{PT} over long time, because of the lower total quantity of hydrate in-place at lower initial saturations. Q_R decreases to a very low level ($Q_R < 0.6$ ST m^3/day/m of well) at $t = 7\,600$ days for the lowest $S_{H0} = 0.30$, and the corresponding hydrate dissociation percentage shown in Figure 12 rises above 0.98, which indicate that almost all the hydrate in the deposit disappears at that time. In the $S_{H0} = 0.44$ and 0.60 cases, there is still hydrate in the deposit at the end of the production periods ($t = 30$ years).

In Figure 13, in the initial period of the production process, the water production rate Q_W increases with a decreasing S_{H0} (corresponding to a larger S_A). While the effect of Q_{PT} is weaker than that of the Q_W dependence on S_{H0} (Q_{PT} and Q_W both increase with decreasing S_{H0}), R_{GW} decreases with the decrease of S_{H0} at early times of the production process. After a long production time, both Q_{PT} and R_{GW} decrease with decreasing S_{H0}. In general, more gas is produced for higher S_{H0}. Additionally, the gas-to-water ratio R_{GW} is favored by a high S_{H0}.

5.2. Sensitivity to the Intrinsic Permeability *k*. Figures 14 and 15 show, respectively, the dependences of (a) Q_{PG}, Q_{PT},

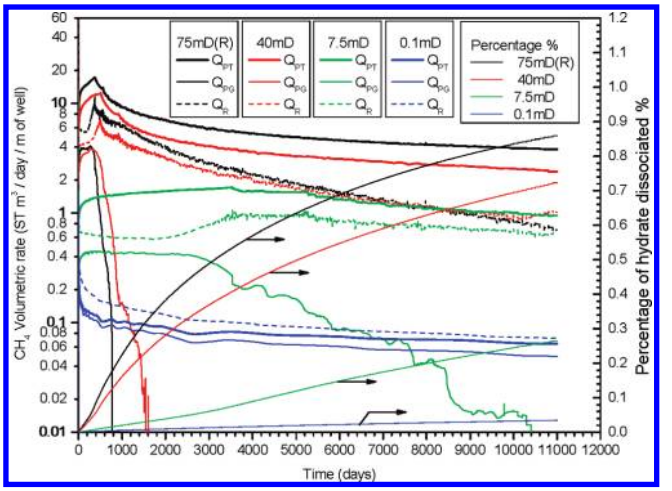

Figure 14. Sensitivity analysis: effect of k on Q_{PG}, Q_{PT}, Q_R and the percentage of hydrate dissociated when $\Delta P_W = 0.2P_0$ during gas production from the methane hydrate deposit at the SH7 Site of the Shenhu Area, South China Sea ($k = 75$ mD in the reference case).

Q_R, and the percentage of hydrate dissociated in the HBL and (b) Q_W and R_{GW} on the intrinsic permeability k of the domain (including the HBL, overburden, and underburden) for the $\Delta P_W = 0.2P_0$ case.

Reducing k from 75 to 0.1 mD results in significant deterioration of gas production performance. In the long term, Q_{PT} is reduced from about 4.0 ST m^3/day/m of well for $k = 75$ mD to less than 0.1 ST m^3/day/m of well when $k = 0.1$ mD (Figure 14). In the $k \leq 75$ mD cases, there are still hydrates in the deposit after 30 years of production.

The water production rate Q_W shown in Figure 15 also decreases with a decrease of k, and this positive effect is dominant comparing with the gas production reduction. In other words, a declining k is favorable for the relative criterion of production performance R_{GW} (Figure 15). There is continuous gas escape via the overburden, caused by the limited confinement effect of the boundaries, and a continuous influx of water through the boundaries (including both the overburden and underburden) during the production procedure in this study. The gas production rate Q_{PT} is affected by the permeability of the overburden rather than

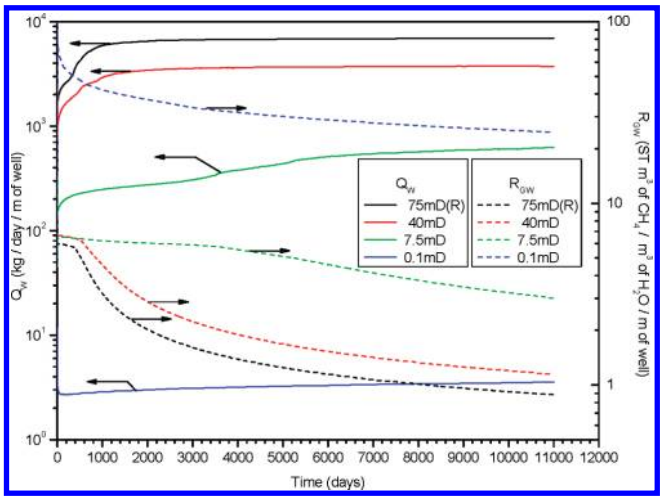

Figure 15. Sensitivity analysis: effect of k on the evolution Q_W and R_{GW} when $\Delta P_W = 0.2P_0$ during gas production from the methane hydrate deposit at the SH7 Site of the Shenhu Area, South China Sea (k = 75 mD in the reference case).

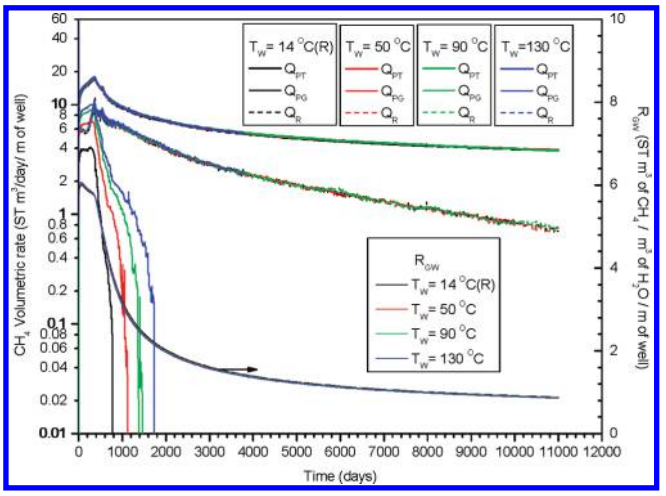

Figure 16. Sensitivity analysis: effect of T_W on Q_{PG}, Q_{PT}, Q_R, and R_{GW} when $\Delta P_W = 0.2P_0$ during gas production from the methane hydrate deposit at the SH7 Site of the Shenhu Area, South China Sea (T_W = 14 °C in the reference case).

underburden, while the water production rate Q_W decreases with the decrease in k of both of them.

5.3. Sensitivity to T_W. Figure 16 shows the dependences of Q_{PG}, Q_{PT}, Q_R, and R_{GW} on the temperature of the circulating hot water in the well (T_W = 50, 90, 130 °C) for the $\Delta P_W = 0.2P_0$ case. In the reference case, T_W = 14 °C, i.e., very close to the initial HBL temperature at the location (elevation) of the well.

With an increase in T_W from 14 to 130 °C, both the total gas production rate Q_{PT} and the rate of the gas released from hydrate dissociation Q_R increased very slightly (Figure 16). Thus, the higher T_W appears to have a limited (to practically no) effect on gas production, confirming the results of an earlier study.[28] One of the reasons for this is the limited efficiency of conduction as the main heat transfer mechanism, with the rate of its propagation declining significantly over time as the volume around the well increases as a function of r^2.[20] Furthermore, the opposite direction of the conductive and advective heat flows, from the well to the deposit and from the HBL toward the well as part of the fluid flow, during the production process confines the heat stimulation effect to a very limitied zone around the well.

In Figure 16, the volumetric rate of CH_4 production in the gas phase Q_{PG} increases with increasing T_W. As already discussed in the T_W = 14 °C cases of Figures 4 and 8, the gas produced in the gas phase Q_{PG} decreases to less than 0.01 ST m^3/day/m of well at about t = 800 days, with most of the free gas in the deposit accumulating early in the cylindrical zone around the well. In Figure 16, (a) the maximum of Q_{PG} and (b) the time to reach Q_{PG} < 0.01 ST m^3/day/m of well increases with increasing T_W, because most free gas is accumulated in the cylindrical zone around the well, where the local S_H and S_G are significantly affected by T_W. The higher the T_W, the more hydrate dissociated and gas accumulates in this zone, leading to higher Q_{PG} and a slower Q_{PG} decline. The gas-to-water ratios R_{GW} appear practically insensitive to T_W because of the limited overall effect of T_W on dissociation.

5.4. Sensitivity to T_0. Figure 17 shows the $P-T$ equilibrium relationship in the phase diagram of the water−CH_4−hydrate system. In this study, the T_0 sensitivity analysis is investigated through the following two cases: (i) T_0 is reduced by approximately 2.5 °C (from T_0 = 13.7 °C at the well location in the

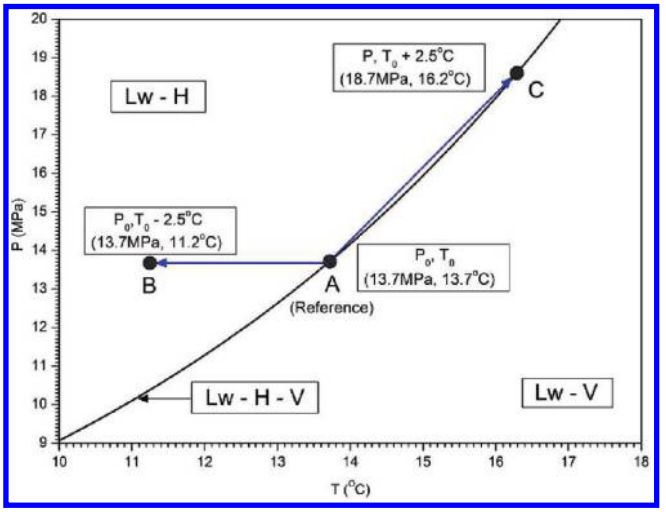

Figure 17. Phase diagram of the water−CH_4−hydrate system: the cases investigated in the analysis of sensitivity of production to the initial reservoir temperature T_0.

reference case to $T_0 - 2.5$ = 11.2 °C), while keeping the same geothermal gradient and P equal to P_0 = 13.7 MPa in the reference case; (ii) T_0 is increased by approximately 2.5 °C (from T_0 = 13.7 °C at the well location to $T_0 + 2.5$ = 16.2 °C), the geothermal gradient remains unchanged, and P is increased to the corresponding equilibrium P_{eq} = 18.7 MPa (reflecting a deeper, warmer deposit). Cases (i) and (ii) are, respectively, represented by points B and C in Figure 17, while the reference case is point A.

Figure 18 shows the dependences of Q_{PG}, Q_{PT}, Q_R, and R_{GW} on the hydrate stability, as quantified by the initial temperature T_0 in the HBL at z = 0 (the position of the production well). As discussed above, in the reference case, the initial pressure P_B at the base of the HBL is slightly higher than the equilibrium pressure corresponding to T_B, and it is relatively easy to destabilize the hydrate with mild depressurization. In Figure 18, the colder and more stable system (T_0 − 2.5 = 11.2 °C) results in consistently lower Q_{PT}. As expected, over the first 10 years, Q_R in the colder system (T_0 − 2.5) is lower than that in the reference case (T_0), which indicates that the hydrate dissociation is reduced in the

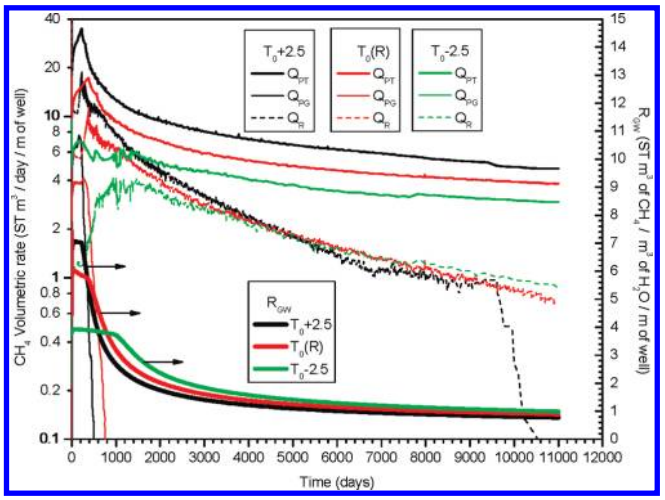

Figure 18. Sensitivity analysis: effect of lower T_0 on Q_{PG}, Q_{PT}, Q_R, and R_{GW} when $\Delta P_W = 0.2P_0$ during gas production from the methane hydrate deposit at the SH7 Site of the Shenhu Area, South China Sea (P_0 = 13.7 MPa, T_0 = 13.7 °C in the reference case).

colder system. After 10 years, Q_R in the colder system ($T_0 - 2.5$) is slightly higher, because more hydrate remains undissociated in the deposit (i.e., there is more hydrate available to dissociate) in the colder system at long times. The difference between Q_{PT} and Q_R in the colder system ($T_0 - 2.5$) is smaller than that in the reference case, especially when Q_R is almost the same after 10 years because the effective permeability k_{eff} is lower in the presence of more hydrate within the deposit in the colder system. The R_{GW} shows a different dependence on T_0 over time in Figure 18, indicating lower initial gas production in the more stable (colder) system and slightly higher R_{GW} after about 3 years. For a given ΔP_W, the higher the T_0 (and the closer to the equilibrium temperature) in the hydrate deposit, the better the reservoir performance is in terms of both gas production (increasing) and water production (decreasing).

The characteristics of the curve profiles of (a) Q_{PG}, Q_{PT}, Q_R, and (b) R_{GW} in the deeper and warmer system (P_0 = 18.7 MPa, T_0 = 16.2 °C) in Figure 18 show a similar dependence on T_0. Thus, a higher T_0 leads to initially larger Q_{PT} and Q_W and larger Q_R and R_{GW}. In this case, the Q_R ($T_0 + 2.5$) decreases rapidly at about t = 9 600 days, indicating the disappearance of hydrate in the deposit. In the reference case (Figure 7), the hydrates in the deposit are not exhausted even at t = 30 years. In general, the deposit with higher initial temperature is a more desirable production target.

6. Summary and Conclusions

In this work, we investigated the gas production potential from marine gas hydrate deposits at site SH7, in the Shenhu Area of the South China Sea, during the China Geological Survey of 2007. From the numerical simulation results, the following conclusions are drawn: (1) On the basis of the field measurement of the hydrate sample from site SH7 (including the temperatures at the different depth of the deposit), the local geothermal gradient, the equilibrium pressure at the base of the hydrate layer, and the general tendency of hydrate deposits to follow the hydrostatic gradient, the initial conditions in the hydrate deposit in this study were calculated and the system was brought to equilibrium. (2) During the modeled 30 years of continuous production, Q_{PT} exceeded Q_R in all the cases with a different driving force ΔP_W, and Q_{PG} was much smaller than Q_{PT}, which indicated that the majority of the produced gas came from CH_4 dissolved in water rather than from the free gas phase. A local maximum of Q_{PT} = 17.3 ST m^3/day/m of well is reached, before a decline begins at about t = 390 days in the reference case ($\Delta P_W = 0.2P_0$), and the corresponding Q_R shows the similar profile as Q_{PT}. (3) In the reference case, for a well spacing of 90 m and a horizontal well with the length of 1000 m, the Q_{PTmax} for the entire deposit reaches 3.46×10^4 ST m^3/day (1.22 MMSCFD), which is over 7 times lower than the rule-of-thumb for commercially viable production rates from offshore gas wells. The corresponding water production rate is about $Q_W = 1.2 \times 10^7$ kg/day (1.2×10^4 ton/D), which is unmanageable, and R_{GW} is prohibitively low (R_{GW} < 5 ST m^3 of CH_4/m^3 of H_2O/m of well). (4) In this study, the dissociation is characterized by the following features: evolution of the initial cylindrical hydrate dissociation interface around the well, evolution of the upper and lower dissociation interfaces at the top and the bottom of the hydrate layer, the mergence of the lower and the cylindrical interfaces, which is earlier than that of the upper and cylindrical interfaces, and gas accumulation initially around the well within the cylindrical dissociated zone and immediately below the lower dissociation interface at later times of the production periods. (5) The temperature distribution in the deposit confirmed the earlier conclusion that there is fluid flow from both the upper and lower boundaries. The disappearance of the low-T zone above the well (caused by hydrate dissociation) indicates the relatively warmer water flows and heat flows from the overburden (where there is an inversion of geothermal gradient because of dissociation-induced cooling in the HBL). Also, the temperature increase immediately below the well is caused by the warmer water rising from the underburden. (6) The analysis of sensitivity to S_{H0} indicated that the maximum of the total gas production rate Q_{PT} increased initially with a decrease in S_{H0} but declined in the long run with a decrease in S_{H0} because of a leaner resource. In general, a higher S_{H0} is associated with a higher gas production and a more favorable R_{GW}. (7) Sensitivity analysis indicated that significant deterioration of gas production performance is observed with a declining intrinsic permeability k of the deposit (including the overburden, the HBL, and the underburden) despite an improvement in the R_{GW} performance. (8) The analysis of sensitivity to the temperature of the circulating hot water in the well T_W indicates that the higher T_W has a practically negligible effect on gas production performance, with practically no impact on both Q_{PT} and R_{GW}. This indicates that of the combination of depressurization and thermal stimulation that is possible in the well design used in this study, depressurization is the only active dissociation method, thus confirming earlier observations about its superior effectiveness (be orders of magnitude[5]). The reason for this is the narrow effective range of T_W around the well, caused by the limited efficiency of conduction as the main heat transfer mechanism and the opposite direction of the conductive and advective heat flows. (9) The analysis of sensitivity to the initial temperature in the middle of the HBL T_0 indicates that deeper, warmer deposits have consistently a higher production potential, but this does not mean that they can attain commercially viable performance. (10) After conducting a thorough sensitivity analysis involving reasonable system parameters and conditions, it appears that the hydrate accumulations at the SH7 site of the Shenhu Area in the South China Sea do not

appear to be promising candidates for gas production when using current horizontal well technology.

Acknowledgment. This work was supported by National Natural Science Foundation of China (Grants 20773133, 51004089, and 51076155), CAS Knowledge Innovation Program (Grant KGCX2-YW-3X6), Science & Technology Program of Guangdong Province (Grant 2009B050600006), and CAS Magnitude Science and Technology Apparatus Development Program (Grant YZ200717), which are gratefully acknowledged. The contribution of G. J. Moridis was supported by the Assistant Secretary for Fossil Energy, Office of Natural Gas and Petroleum Technology, through the National Energy Technology Laboratory, under the U.S. Department of Energy, Contract No. DE-AC02-05CH11231. The authors are indebted to Matt Reagan and Dan Hawkes for their insightful comments.

Nomenclature

C = specific heat (J/kg/K)
k = intrinsic permeability (m^2)
k_{eff} = effective permeability (m^2)
k_{rA} = aqueous relative permeability (m^2)
k_{rG} = gas relative permeability (m^2)
k_Θ = thermal conductivity (W/m/K)
$k_{\Theta RD}$ = thermal conductivity of dry porous medium (W/m/K)
$k_{\Theta Rw}$ = thermal conductivity of fully saturated porous medium (W/m/K)
$k_{\Theta I}$ = thermal conductivity of ice (W/m/K)
M_W = the cumulative mass of the produced water (m^3 of H_2O)
P = pressure (Pa)
P_B = initial pressure at base of HBL (Pa)
P_0 = initial pressure in the middle of HBL (Pa)
P_W = pressure at the well (Pa)
P_Q = pressure at the quadruple point (Pa)
$Q_{PD} = Q_{PT} - Q_{PG}$ (ST m^3/day/m of well)
Q_W = mass rate of aqueous phase production at the well (kg/day/m of well)
Q_{PG} = volumetric rate of CH_4 production at the well in the gas phase (ST m^3/day/m of well)
Q_{PT} = volumetric rate of total CH_4 production at the well (ST m^3/day/m of well)
Q_R = volumetric rate of CH_4 release from hydrate dissociation (ST m^3/day/m of well)
r = radius (m)
R_{GW} = the gas to water production ratio (ST m^3 of CH_4/m^3 of H_2O/m of well)
S = phase saturation
t = times (days)
T = temperature (°C)
T_B = initial temperature at base of HBL (°C)
T_{0F} = temperature at the ocean floor (°C)
T_0 = initial temperature in the middle of HBL (°C)
V_P = the cumulative volume of the produced CH_4 (ST m^3 of CH_4)
x,y,z = Cartesian coordinates (m)
X_S = salinity
ΔP_W = driving force of depressurization, $P_0 - P_W$ (Pa)
Δx = discretization along the x-axis (m)
Δz = discretization along the z-axis (m)
ΔZ_H = HBL thickness (m)
ΔZ_O = overburden thickness (m)
ΔZ_U = underburden thickness (m)
ΔZ_W = well position above the HBL base (m)
ϕ = porosity
ρ_R = grain density (kg/m^3)
λ = van Genuchten exponent, Table 2

Subscripts and Superscripts

0 = denotes initial state
A = aqueous phase
B = base of HBL
cap = capillary
e = equilibrium conditions
G = gas phase
H = solid hydrate phase
I = ice phase
irA = irreducible aqueous phase
irG = irreducible gas
n = permeability reduction exponent, Table 2
n_G = gas permeability reduction exponent, Table 2
O = overburden
P = production stream
R = rock
S = salinity
U = underburden
W = well